Biodegradable Poly(glycolic acid) Nanofiber Prepared by CO_2 Laser Supersonic Drawing

Akihiro Suzuki, Rio Shimizu

Interdisciplinary Graduate of School of Medicine and Engineering, University of Yamanashi, Takeda-4, Kofu 400-8511 Japan

Received 28 September 2010; accepted 1 December 2010
DOI 10.1002/app.33982
Published online 31 March 2011 in Wiley Online Library (wileyonlinelibrary.com).

ABSTRACT: Biodegradable Poly(glycolic acid) (PGA) nanofibers were prepared by irradiating a PGA fiber with radiation from a carbon dioxide (CO_2) laser while drawing it at supersonic velocities and was collected as a nonwoven. A supersonic jet was generated by blowing air into a vacuum chamber through the fiber injection orifice. The flow velocity from the orifice was estimated by computer simulation; the fastest flow velocity was calculated to be 401 m s^{-1} at a chamber pressure of 6 kPa. A nanofiber obtained using a laser power of 10 W and a chamber pressure of 6 kPa had an average diameter of 359 nm and a draw ratio of about 77,600. © 2011 Wiley Periodicals, Inc. J Appl Polym Sci 121: 3078–3084, 2011

Key words: poly(glycolic acid); (PGA); nanofibers; carbon dioxide laser supersonic drawing; SEM; DSC

INTRODUCTION

Nanofibers have been produced by electrospinning, sea-island-type conjugated melt spinning, single-orifice melt blowing, and jet blowing.[1–15] Electrospinning is the most widely used method for preparing nanofibers. Electrospun nanofibers have been investigated for use as scaffold in tissue engineering because of their large surface area per unit mass and their very small pore size.

Poly(glycolic acid) (PGA) biodegradable material begins to break down by hydrolysis and enzymes, and is widely used in medicine. PGA has diverse biodegradability, good mechanical properties, biocompatibility, and very low solubility in organic solvents.[16–18] Nonwoven PGA fabrics composing of nanofibers have been used extensively in scaffolding matrices for tissue regeneration due to their excellent degradability, good initial mechanical properties and cell viability on the matrices. Nonwoven PGA fabrics have been prepared by electrospinning,[19–21] and electrospun PGA nanofibers were prepared by spraying a solution of PGA-1,1,1,3,3,3 hexafluoro-2-propanol onto a metallic collector under high voltage.

Recently, we proposed a new approach for producing nanofibers. It involves irradiating a fiber with radiation from a carbon dioxide (CO_2) laser while drawing it at a supersonic velocity. A supersonic jet was generated by blowing air into a vacuum chamber through the orifice used to inject the fiber into the vacuum chamber. The adiabatic expansion of air across the orifice cools the jet. The fiber is instantly melted by the high-power laser beam that irradiates the cold supersonic jet. It is then deformed by the shear force generated by the supersonic flow, and ultradrawn to a draw ratio of the order of 10^5. We named this preparation method CO_2-laser supersonic drawing. Supersonic drawing has already been applied to poly(L-lactic acid) (PLLA), poly(ethylene-2,6-naphthalate) and poly(ethylene terephthalate),[22–24] and their nanofibers were obtained without using any solvent or without removing the second component. The nanofiber obtained by the CO_2 laser supersonic drawing is basically endless fiber because a monofilament fiber is continuously drawn by irradiating laser. The CO_2-laser supersonic drawing can easily prepare various nanofibers by only CO_2 laser-irradiation without combining any processes.

In this paper, we prepare PGA nanofibers by CO_2-laser supersonic drawing. The relationships between the drawing conditions and the fiber diameter were determined.

EXPERIMENTAL

The PGA fiber used in the present study is an as-spun fiber with a diameter of 100 μm and a birefringence of 2.6×10^{-3}, and was supplied by GUNZE, Ltd. It was almost isotropic.

Correspondence to: A. Suzuki (a-suzuki@yamanashi.ac.jp).
Contract grant sponsor: Japan Society for the Promotion of Science.

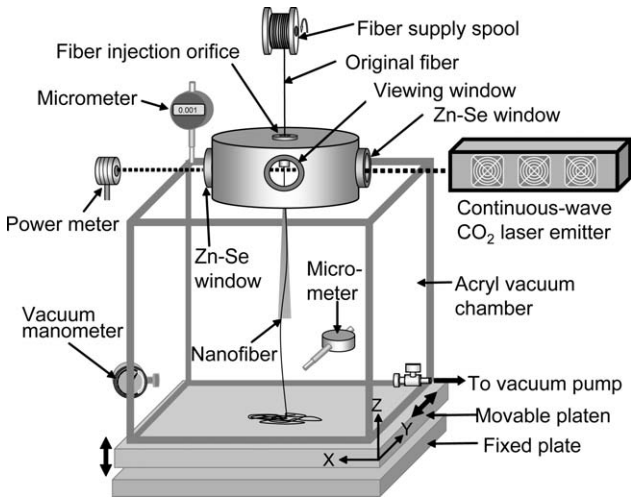

Figure 1 Schematic diagram of the apparatus used for CO_2-laser supersonic drawing.

The morphology of the produced nanofiber was determined by scanning electron microscopy (SEM) (JSM-6060LV, JEOL Ltd.) using an accelerating voltage of 10 kV. Before SEM observation, the samples were coated with gold using a sputter coater. The average diameter and the diameter distribution of the nanofiber were measured using an imaging analyzer. The average diameter of a fiber was determined by averaging the diameter of 100 locations along the fiber.

The DSC measurements were carried out using a THERM PLUS 2 DSC 8230C calorimeter (Rigaku Co.). The DSC scans were performed within the temperature range of 25–250°C, using a heating rate of 10°C min^{-1}. All DSC experiments were carried out under a nitrogen purge. The DSC instrument was calibrated with indium. The degree of crystallinity (X_c) was determined by fusion heat (ΔH_m) and enthalpy of cold crystallization (ΔH_{cc}) as follows:

$$X_c(\%) = \frac{\Delta H_m + \Delta H_{cc}}{-139} \times 100 \qquad (1)$$

where -139 J g^{-1} is used as the fusion heat of the crystalline phase of PGA.[25]

Figure 1 shows the apparatus used for the CO_2-laser supersonic drawing. It consists of a spool to supply the fiber, a continuous-wave CO_2 laser with an output wavelength of 10.6 μm and a maximum power of 30 W, an acrylic vacuum chamber with Zn-Se windows and a 0.5-mm-diameter orifice for injecting the fiber, a power meter, a movable platen, and a vacuum pump. The vacuum chamber was placed on the movable platen that consisted of a micro-alignment stage and a lab jack that can be moved parallel to the *Y* and *Z* axes allowing the laser irradiation point on the fiber to be finely adjusted.

The velocity distribution from the orifice and the force exerted on the fiber in the air jet were estimated by performing fluid analysis using a three-dimensional (3D) finite element method (FEM) with ANSYS® CFZ 11.0 software.

RESULTS AND DISCUSSION

When performing CO_2-laser supersonic drawing using an air jet, it is very important to determine the velocity distribution in the air jet and the force that is exerted on the fiber surface. Shear force is applied to the fiber in the supersonic jet in the fluid flow direction and simultaneously a compressive force is also applied in the vertical direction because the air flow acts like a viscous fluid. The resultant force acts as the drag force to draw the molten fiber to a draw ratio of the order of 10^5 and it determines the fiber's diameter and its superstructure. To elucidate the supersonic drawing mechanism it is necessary to analyze the forces applied to the fiber in the air jet.

Figure 2 shows the flow velocity distribution of the air jet in the XZ-plane calculated by the 3D FEM. This simulation was performed for a chamber pressure of 6 kPa and a 100-μm-diameter fiber centered on a 0.5-mm-diameter orifice. The flow from the orifice was generated by blowing air into the vacuum chamber to produce a supersonic jet that does not have any accompanying flow that would make the air flow turbulent. This stable airflow generates a speedy current that enables the fiber to be irradiated by the laser beam without causing it to swing. The fastest flow velocities are produced about 3 mm below the orifice and are in the range 363 and 403 m sec^{-1}, making

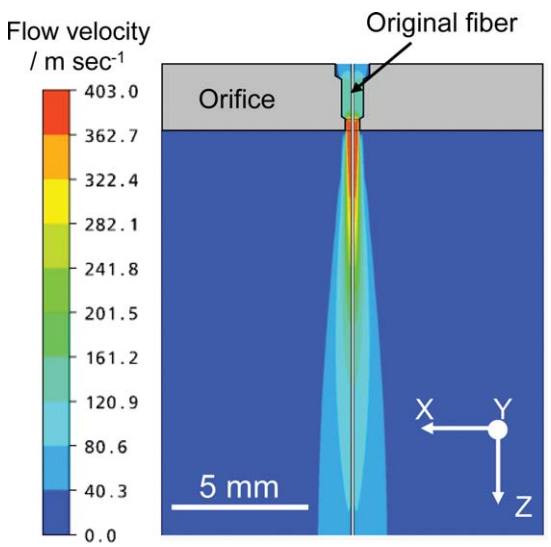

Figure 2 Flow velocity distribution of the air jet in the XZ-plane obtained by the FEM. [Color figure can be viewed in the online issue, which is available at wileyonlinelibrary.com.]

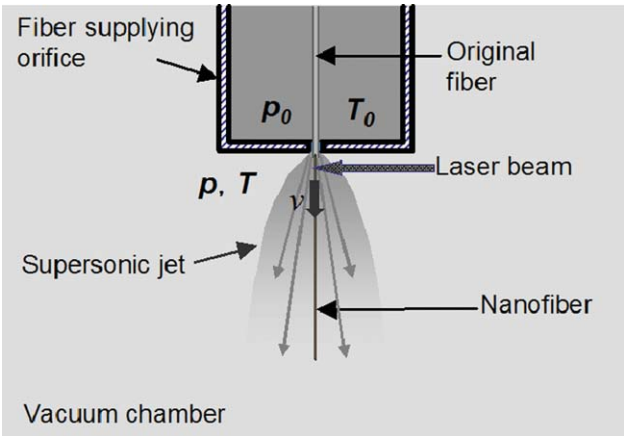

Figure 3 Schematic diagram of free air expansion into vacuum chamber. [Color figure can be viewed in the online issue, which is available at wileyonlinelibrary.com.]

them supersonic. As the distance from the orifice increases, the flow velocity along the fiber decreases rapidly.

Figure 3 shows the schematic diagram for free expansion of air in the supersonic jet. The air flow from the orifice occurred by the pressure difference across the orifice when the vacuum chamber was exhausted by the vacuum pomp. The adiabatic expansion of air across the orifice cools the jet. Since the conservation of energy applies along streamlines, the following relation holds between the ratio of the temperature before adiabatic expansion (T_0) to the temperature after adiabatic expansion (T) and the Mach number (M)[26]

$$\frac{T}{T_0} = \left\{1 + \frac{(\gamma - 1)M^2}{2}\right\}^{-1} \tag{2}$$

where γ ($=C_p/C_v$) is the ratio of heat capacity at a constant pressure (C_p) to that of a constant volume (C_v); in the case of air, γ is 1.4 because it consists primarily of diatomic gases. The flow velocity is converted into a Mach number by dividing it by the sonic speed at a temperature of T_0:

$$M = \frac{v}{C} = \frac{v}{331.5 + 0.6(T_0 - 273.5)} \tag{3}$$

TABLE I
Flow Velocity (v), Mach Number (M), Temperature (T) in the Supersonic Jet at Four Different Chamber Pressures (p_{ch})

p_{ch}/kPa	v/m s^{-1}	M at 298.5 K	T/K
50	295	0.9	261
30	348	1.0	249
20	372	1.1	243
6	402	1.2	235

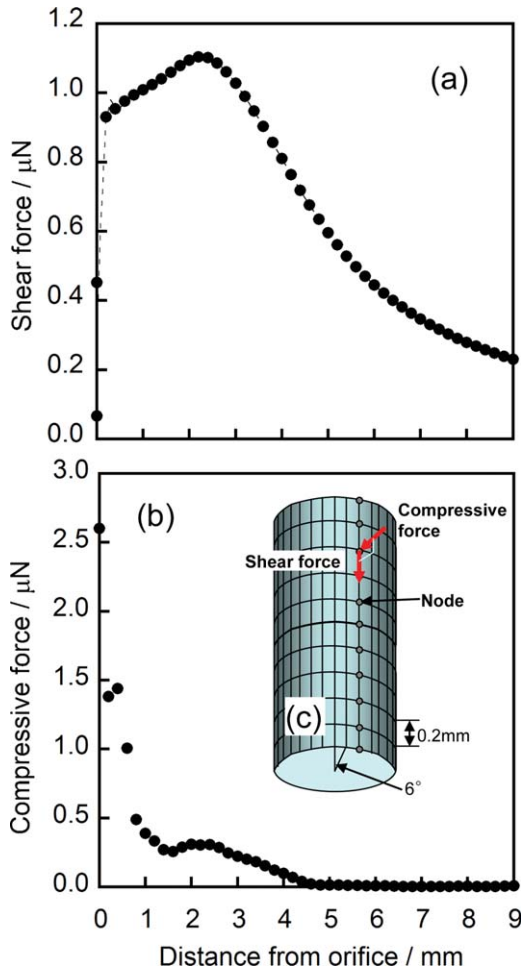

Figure 4 Variation in the (a) shear force and (b) compressive force at the node of the fiber surface in the Z-axis direction at a distance from the orifice, and (c) the 3D model used to simulate the shear force and the compressive force. [Color figure can be viewed in the online issue, which is available at wileyonlinelibrary.com.]

Table I lists the flow velocity (v), Mach number, and temperature (T) in the supersonic jet for four different chamber pressures. The flow velocity exceeds the speed of sound only at chamber pressures under 30 kPa. The Mach number at a chamber pressure of 6 kPa is 1.2. The temperature (T) of the supersonic jet at Mach 1.2 is as low as 235 K.

To estimate the drag force acting on the fiber in the supersonic jet, the forces parallel and perpendicular to the surface of the fiber (the shear force and the compressive force, respectively) were analyzed by the 3D FEM. Figure 4 shows the variation in (a) the shear force and (b) the compressive force which is exerted on the fiber surface in the Z-axis direction as a function of distance from the orifice, and (c) the 3D model used to simulate these forces. To clarify, the shear force and the compressive force are the values at the nodes along the fiber axis in Figure 4(c). As the distance from the orifice

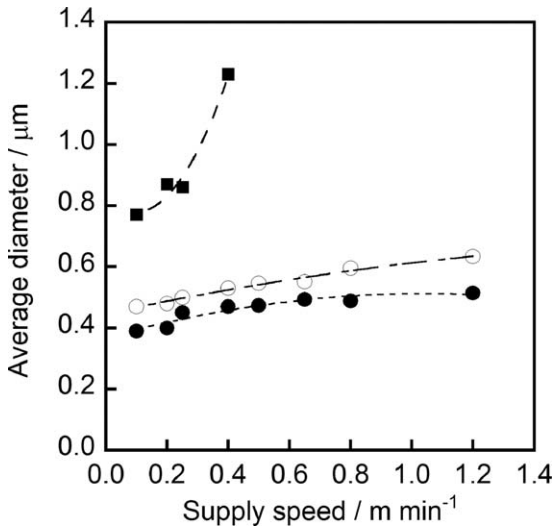

Figure 5 Variation in the average diameters of the fibers obtained at three different chamber pressures (p_{ch}) and a laser power of 8W with supply speed, ●: $p_{ch} = 6$ kPa, ○: $p_{ch} = 10$ kPa, and ■: $p_{ch} = 20$ kPa.

increases, the shear force decreases rapidly after reaching a maximum value at a distance of 2.2 mm from the orifice. The compressive force is greatest at the origin and decreases rapidly with increased distance away from the orifice. The shear force and the compressive force are simultaneously high at a distance of about 3 mm from the orifice. The result of the shear force and the compressive force is critical for supersonic-drawings of molten fiber heated by a high-power laser beam.

The experimental factors that determine the fiber diameter are the laser power, the chamber pressure, the fiber supply speed, and the laser beam irradiation position. First, the effect of the laser irradiation position on the fiber diameter was confirmed by a preliminary experiment. It is very important to investigate this because the shear force and the compressive force depend strongly on the distance from the orifice as shown in Figure 4. The average diameter increases as the laser irradiation position is moved away from the orifice because the shear force decreases rapidly as the distance from the orifice increases. To obtain a thinner nanofiber, it is necessary to irradiate the fiber with a higher laser power at a position where a higher drag force is generated. The laser irradiation position was kept constant at a position obtained by the thinnest nanofiber during a series of experiments.

Next, the effects of the laser power, the chamber pressure, and the fiber supply speed on the fiber diameter were investigated.

Figure 5 shows the dependence of the average fiber diameter on supply speed at three different chamber pressures. The laser power was held constant at 8 W during this series of experiments. As the supply speed decreases, the average diameter at each chamber pressure decreases; it is less than 1 μm at chamber pressures of 6 and 10 kPa (i.e., at a flow velocity of about 390 m s^{-1}) in the supply speed range of 0.1–1.2 m min^{-1}. The thinnest nanofiber obtained at $p_{ch} = 6$ kPa has an average diameter of 388 nm. Reducing the supply speed, reduces the rate at which the polymer mass is moved into the laser irradiation position. The deformation of the molten polymer increases because the same drag force acts on the smaller mass of polymer that is melted by the laser irradiation. A decrease in the chamber pressure, i.e., an increase in the flow velocity, implies an increase in the drag force. A larger drag force induces a higher plastic flow rate, resulting in a thinner nanofiber being produced.

Figure 6 shows the diameter distributions of the fibers obtained at four different supply speeds (S_s), a laser power of 8 W, and a chamber pressure of 6 kPa. As the supply speed decreases, the diameter distribution gradually becomes narrower, and the

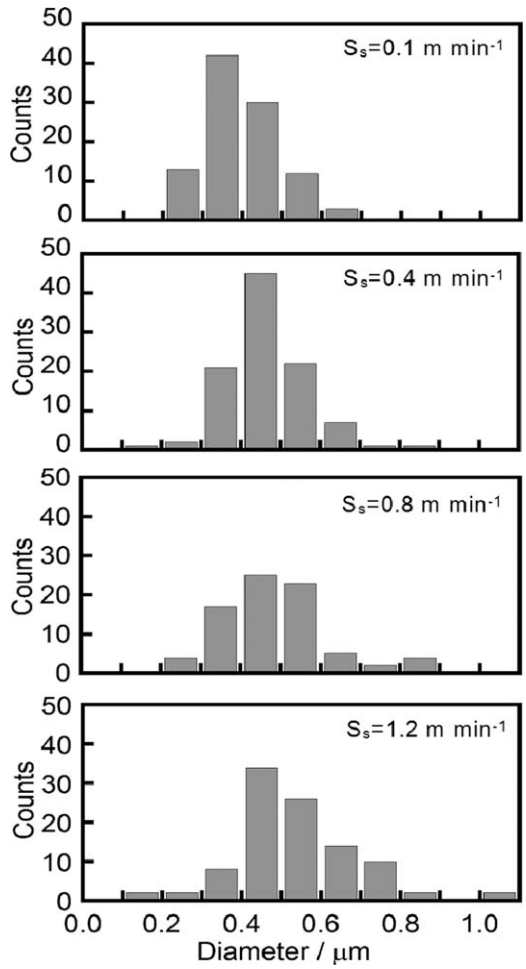

Figure 6 Diameter distributions for the fibers obtained at three different supply speeds (S_s) chamber pressures (p_{ch}) of 6 kPa, and a laser power of 8 W.

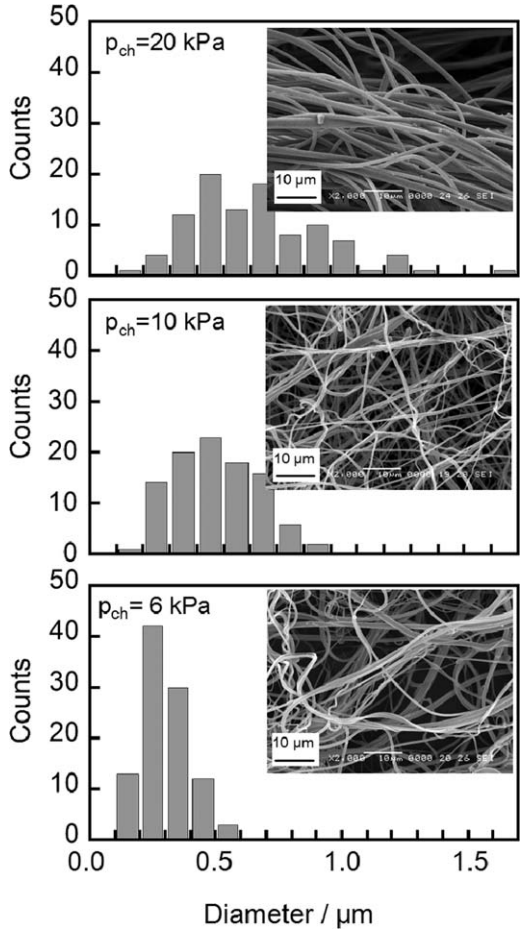

Figure 7 Diameter distributions and SEM photographs at ×2000 magnification for the fibers obtained at three different chamber pressures (p_{ch}), a supply speed of 0.1 m min^{-1}, and laser power of 8 W.

average diameter decreases. The thinner the fiber diameter, the higher the uniformity becomes.

Figure 7 shows diameter distributions and SEM photographs at 2000× magnification for the fibers obtained at three different chamber pressures (p_{ch}), a supply speed of 0.1 m min^{-1}, and a laser power of 8 W. The thinnest nanofiber obtained at $p_{ch} = 6$ kPa has the narrowest diameter distribution. As the chamber pressure decreases, the diameter distribution gradually becomes narrower, and the average diameter decreases. The thinnest nanofiber produced had an average diameter of 388 nm, a minimum diameter of 240 nm, a maximum diameter of 670 nm, and a standard deviation of 0.096. The thinner the fiber diameter, the higher the uniformity became.

The SEM micrographs reveal that the nanofiber has a smooth surface that has not been roughened by laser ablation and does not have droplets.

Next, the effect of laser power on the fiber diameter was examined. Figure 8 shows the variation in the average fiber diameter with the supply speed for three different laser powers. As the supply speed is reduced, the fiber diameter at each laser power decreases, and the nanofiber with an average diameter of 359 nm was obtained when the fiber was moved into position at a speed of 0.1 m min^{-1} and was irradiated with a laser power of 10 W. Irradiating at a higher laser power instantly reduces the polymer viscosity, causing the polymer flow rate to increase.

The draw ratio (λ) can be calculated easily using the following equation:

$$\lambda = \left(\frac{d_0}{d}\right)^2, \tag{4}$$

where d_0 is the diameter of the original fiber and d is that of the nanofiber, and the volumes before and after drawing are assumed to be equal. The estimated draw ratio of the thinnest nanofiber is about 77,600. A very large plastic deformation occurs momentarily during CO_2-laser supersonic drawing.

Figure 9 shows SEM micrographs at 2000× magnification for fibers obtained by varying laser power at a chamber pressure of 6 kPa and a supply speed of 0.1 m min^{-1}. As the laser power is increased, a reduction in diameter is confirmed visually by SEM micrographs. The SEM micrographs reveal that the nanofiber has a smooth surface that has not been roughened by laser ablation and does not have droplets.

Figure 10 shows DSC curves of the original fiber and the nanofibers obtained at three different laser powers (P_L), a supply speed of 0.1 m min^{-1}, and a chamber pressure of 6 kPa. Table II lists the cold crystallization temperature (T_{cc}), melting temperature (T_m), enthalpy of cold crystallization (ΔH_{cc}), fusion heat (ΔH_m), and the degree of crystallinity

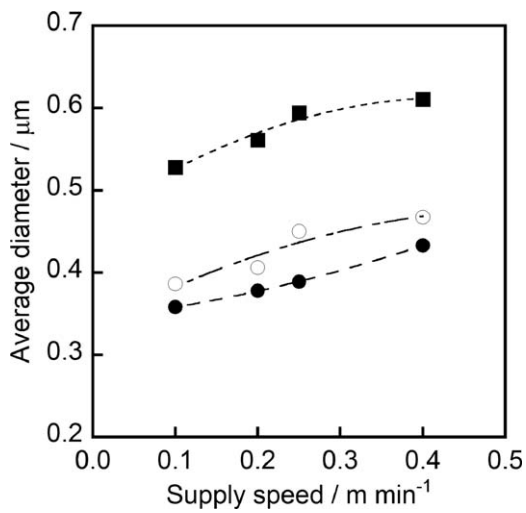

Figure 8 Variation in the average diameter of fibers obtained at three different laser powers (P_L) with supply speed, ■: $P_L = 5$ W, ○: $P_L = 8$ W, and ●: $P_L = 10$ W.

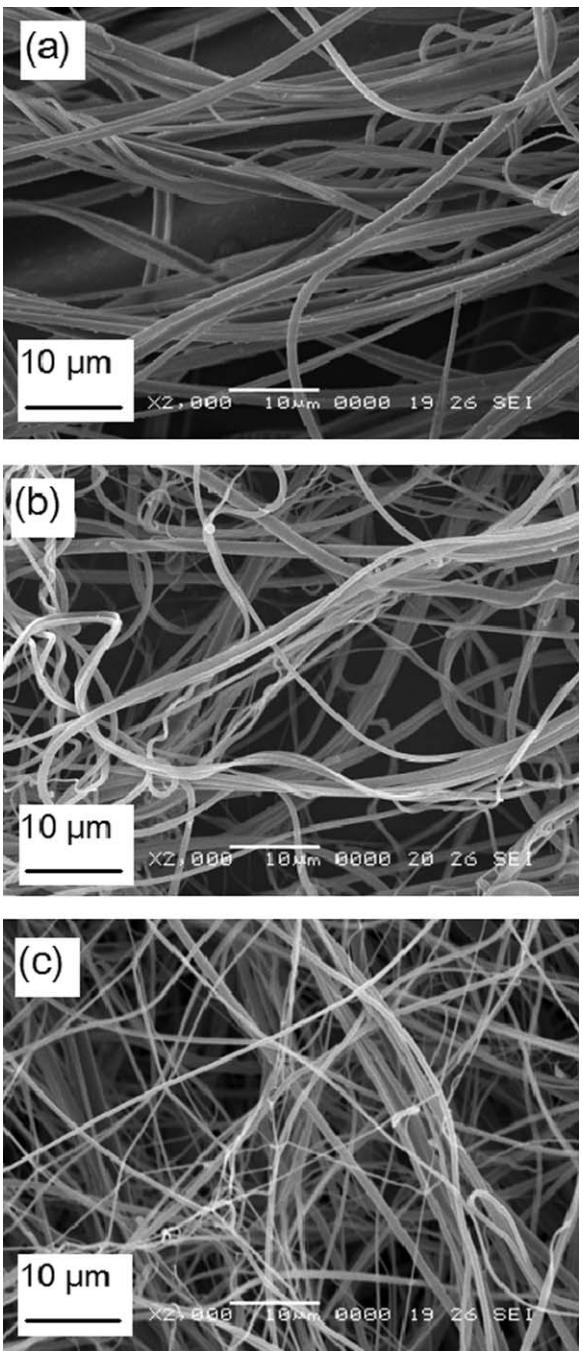

Figure 9 SEM photographs at ×2000 magnification for nanofibers obtained at three different laser powers of (a) 5 W, (b) 8 W, and (c) 10 W, a supply speed of 0.1 m min^{-1} and chamber pressure of 6 kPa.

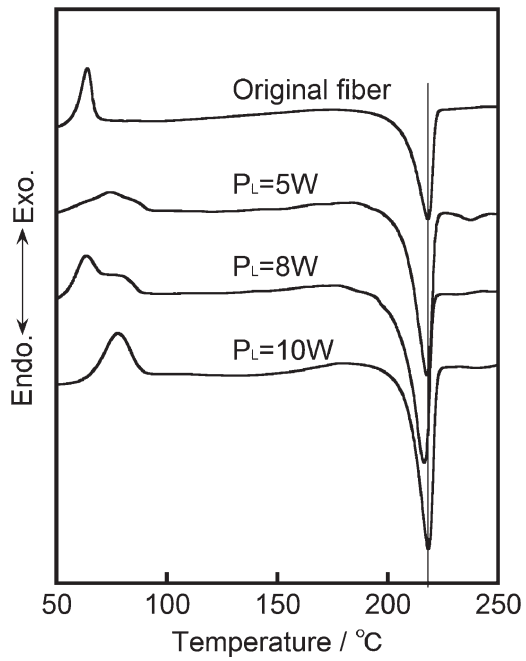

Figure 10 DSC curves of the original fiber and nanofibers obtained at three different laser powers (P_L), a supply speed of 0.1 m min^{-1}, and chamber pressure of 6 kPa.

(X_c) estimated from ΔH_{cc} and ΔH_m for them. All the nanofibers and the original fiber exhibit a broad melting endothermic peak at about 218°C. The melting peaks can be attributed to the melting of crystal formed through flow-induced crystallization by laser irradiation or the melting of the crystal recrystallized during the DSC measurements.[27]

The original fiber has a single exothermic peak of 64°C due to cold crystallization. The nanofibers produced at $P_L = 5$ and 8 W have exothermic peaks at 74 and 64°C, respectively. In addition, there appears to be a shoulder on the high temperature side of each peak. The shoulders in the nanofibers produced at $P_L = 5$ and 8 W are observed at the same temperature as the T_{cc} of the nanofiber produced at $P_L = 10$ W. The nanofiber obtained at $P_L = 10$ W has a single exothermic peak at 78°C.

The shifting of T_{cc} to higher temperatures and the appearance of the shoulder on the high temperature side of the cold crystallization peak show that the crystallization of amorphous chains in the obtained

TABLE II
Cold Crystallization Temperature (T_{cc}), Melting Temperature (T_m), Enthalpy of Cold Crystallization (ΔH_{cc}), Heat of Fusion (ΔH_m), and the Degree of Crystallinity (X_c) Estimated from ΔH_{cc} and ΔH_m for the Original Fiber and the Nanofibers Obtained at Various Laser Powers (P_L), S_s = 0.1 m min^{-1}, and Chamber Pressure of 6 kPa

P_L / W	T_{cc} /°C	T_m /°C	ΔH_{cc} / J g^{-1}	ΔH_m / J g^{-1}	X_c/%
Original	64	218	15.44	−56.01	29
At $P_L = 5$	74	218	19.79	−83.92	46
= 8	64	217	34.48	−95.93	44
= 10	78	218	26.91	−87.03	43

nanofibers are inhibited due to the crystallites formed by the flow-induced crystallization during supersonic drawing. The exothermic peak with the shoulder suggests that there is a difference in the degree of restriction of of amorphous chains. In particular, the T_{cc} of the nanofiber produced at $P_L = 10$ W is 14°C higher than that of the original fiber, and it seems difficult to crystallize the amorphous chains because of the higher degree of restriction among them. These results imply that the thermal movement which serves to crystallize amorphous chains is restricted by the physical structure, made of the crystallites induced during laser supersonic drawing.

The obtained nanofibers have a degree of crystallinity above 40%, and their X_c values are about 10% higher than those of the original fiber. The increase in the X_c with the processing suggests that the flow-induced crystallization occurs during the CO_2 laser supersonic drawing because the molten polymer produced by laser-irradiation is rapidly deformed due to the high plastic flow rate.

CONCLUSIONS

The PGA nanofiber with a uniform diameter was continuously produced by CO_2-laser supersonic drawing. CO_2-laser supersonic drawings could easily produce nanofibers by irradiating a high-power laser beam onto as-spun fibers in a supersonic jet. The resulting force generating from the shear force and the compressive force in the supersonic jet acts as a drag force on the partially molten fiber. The thinnest nanofiber produced had a diameter of 359 nm and was obtained when the supersonic drawing was carried out at a laser power of 10 W, a chamber pressure of 6 kPa, and a fiber supply speed of 0.1 m min^{-1}.

CO_2-laser supersonic drawings can be used for all thermoplastic polymers without having to use a solvent and without removing the second component. The nanofibers obtained are endless nanofibers because a fiber supplied at a constant speed became considerably less laser-irradiated. The PGA nanofiber obtained by the CO_2-laser supersonic drawing is suitable in medicine because it can be easily prepared using only CO_2 laser-irradiation without having to use any solvents which are poisonous to the human body. CO_2-laser supersonic drawing is a new method where nanofibers are produced by using only the CO_2 laser.

The authors are grateful to GUNZE, Ltd. for supplying us with PGA fibers.

References

1. Ding, B.; Kimura, E.; Sato, T.; Fujita, S.; Shiratori, S. Polymer 2004, 45, 1895.
2. Gupta, P.; Wilkes, G. L. Polymer 2003, 44, 6353.
3. Ayutsede, J.; Gandhi, M.; Sukigara, S.; Micklus, M.; Chen, H. E.; Ko, F. Polymer 2005, 46, 1625.
4. Fong, H. Polymer 2004, 45, 2427.
5. Kim, J. S.; Reneker, D. H. Polym Eng Sci 1999, 38, 849.
6. Deitzel, J. M.; Kleinmeyer, J.; Harris, D.; Tan, B. N. C. Polymer 2001, 42, 261.
7. Huang, C.; Chen, S.; Reneker, D. H.; Lai, C.; Hou, H. Adv Mater 2006, 18, 668.
8. Pedicini, A.; Farris, R. J. Polymer 2003, 44, 6857.
9. Varabhas, J. S.; Chase, G. G.; Reneker, D. H. Polymer 2008, 49, 4226.
10. Ellison, C. J.; Phatak, A.; Giles, D. W.; Macosko, C. W.; Bates, F. S. Polymer 2007, 48, 3306.
11. Borkar, S.; Gu, B.; Dirmyer, M.; Delicado, R.; Sen, A. N.; Jackson, B. R.; Badding, J. V. Polymer 2006, 47, 8337.
12. Zhmayev, E.; Cho, D.; Joo, Y. L. Polymer 2010, 51, 274.
13. Dalton, P. D.; Grafahrend, D.; Klinkhammer, K.; Klee, D.; Moller, M. Polymer 2007, 48, 6823.
14. Ogata, N.; Shimada, N.; Yamaguchi, S.; Nakane, K.; Ogihara, T. J Appl Polym Sci 2007, 105, 1127.
15. Eduard, Z.; Daehwan, C.; Yong, L. J. Polymer 2010, 51, 4140.
16. Nair, L. S.; Laurencin, C. T. Prog Polym Sci 2007, 32, 762.
17. Sokolsky-Papkov, M.; Agashi, K.; Olaye, A.; Shakesheff, K.; Domb, A. J. Adv Drug Deliv Rev 2007, 59, 187.
18. Lloyd, A. W. Med Device Technol 2002, 13, 18.
19. Kumbar, S. G.; Nukavarapu, S. P.; James, R.; Nair, L. S.; Laurencin, C. T. Biomaterials 2008, 29, 4100.
20. Liao, Y.; Zhang, L.; Gao, Y.; Zhu, Z.-T.; Fong, H. Polymer 2008, 49, 5294.
21. Agarwal, S.; Wendorff, J. H.; Greiner, A. Polymer 2008, 49, 5603.
22. Suzuki, A.; Aoki, K. Euro Polym J 2008, 44, 2499.
23. Suzuki, A.; Yamada, Y. J Appl Polym Sci 2010, 116 1913.
24. Suzuki, A.; Tanizawa, K. Polymer 2009, 50, 913.
25. Cohn, D.; Younes, H.; Marom, G. Polymer 1987, 28, 2018.
26. Hagena, O. F. Surface Sci 1981, 106, 101.
27. Pecorini, T. J.; Hertzberg, R. W. Polymer 1993, 34, 5053.